© 2018 IJSRSET | Volume 4 | Issue 4 | Print ISSN: 2395-1990 | Online ISSN : 2394-4099
Themed Section : Engineering and Technology

Arima Analysis Of Ferroelectric Lithium Niobate ($LiNbO_3$) THIN Films

Muhammad Nur Aidi[1], Ardian Arif Setiawan[2], Mahfuddin Zuhri[2], Husin Alatas[2], and Irzaman[2]

[1]Departmten of Statistics, Faculty of Mathematics and Natural Sciences Bogor Agricultural University,Kampus IPB Dramaga Bogor Indonesia 16680
[2]Departmten of Physics, Faculty of Mathematics and Natural Sciences Bogor Agricultural University, Kampus IPB Dramaga Bogor Indonesia 16680
Email : nuraidi@yahoo.com, muhammadai@apps.ipb.ac.id

Abstract

Studying atomic and molecular structure of $LiNbO_3$ are very important in order to studying the $LiNbO_3$ character itself. ARIMA model could be used to analyzed. The research result showed that FTIR and XRD value on the heated $LiNbO_3$ thin films could be modelled well by ARIMA.

ARIMA models for Lanthanum Oxide (0 %, 5%, 10 %) doped Lithium Niobate were high accuracy models, since R^2 exceeds than 80 % (99 %, 98 %, 99 % for FTIR data and
90 %, 89 %, 87 % for XRD data), all ARIMA model parameters were significant, and predicted data from ARIMA model followed behaviour actual data. FTIR data on Lanthanum Oxide (0%, 5%, 10%) Doped Lithium Niobate could be well predicted by ARIMA (3,0,0) with the equation models are $y_t = 95{,}785 + 2{,}085\, y_{t-1} - 1.679\, y_{t-2} + 0{,}589\, y_{t-3}$, $y_t = 94{,}924 + 2{,}168\, y_{t-1} - 1{,}806\, y_{t-2} + 0{,}612\, y_{t-3}$, $y_t = 96{,}031 + 2{,}124\, y_{t-1} - 1{,}716 y_{t-2} + 0{,}581\, y_{t-3}$, respectively. XRD data on Lanthanum Oxide (0%) Doped Lithium Niobate could be well predicted by ARIMA (4,0,0) with the equation model are $y_t = 20{,}707 + 0{,}763\, y_{t-1} + 0{,}461\, y_{t-2} - 0{,}240\, y_{t-3} - 0{,}044\, y_{t-4}$ and XRD data on Lanthanum Oxide (5%, 10 %) Doped Lithium Niobate could be well predicted by ARIMA (3,0,0) with the equation models are $y_t = 17{,}277 + 0{,}833\, y_{t-1} + 0{,}342\, y_{t-2} - 0{,}239\, y_{t-3}, y_t = 15{,}151 + 0{,}748\, y_{t-1} + 0{,}342\, y_{t-2} - 0{,}155\, y_{t-3}$, respectively.

ARIMA model l for FTIR data is more accurate than ARIMA model for XRD data, since R^2 of ARIMA model of FTIR data is greater than R^2 of ARIMA model of XRD data and MAPE of ARIMA model of FTIR data is lower than MAPE of of ARIMA model of XRD data. Lanthanum oxide doped to Lithium Niobate Increasing of FTIR value that indicated adding Lanthanum Oxide to Lithium Niobate ($LiNbO_3$) can increase absorbing of $LiNbO_3$ and has lowered the XRD that indicated parameter hints of $LiNbO_3$ decreases which influenced by the radius of its contituuent ions.

Key word: ARIMA, Fourier Transform Infrared, X-Ray Diffraction, $LiNbO_3$, Lanthanum oxide

© 2018 IJSRSET | Volume 4 | Issue 4 | Print ISSN: 2395-1990 | Online ISSN : 2394-4099
Themed Section : Engineering and Technology

1. Introduction

Mastery of basic science and thin film technology are essential in the development of materials science in the future. The role of ferroelectric /pyroelectric / piezoelectric of LiNbO3, LiTaO3, BST, PZT and HgCdTe photon sensor materials, GaAs/AlGaAs are very interesting to examine because they can be applied to DRAM, automatic switching, temperature sensors and solar cells. The pyroelectric and piezoelectric materials are sub-groups of ferroelectric materials. Because of these properties, the ferroelectric material through hysteresis and high dielectric values can be applied to automatic switching [1 - 5] switches, dynamic random access memory (DRAM) [6], non-volatile random access memory (NVRAM) 7] and solar cells [8].

While the operating area of the ferreoelectric sensor (which is also pyro electric) at ambient temperature is below the Curie temperature (Tc = 490^{o}C) [9]. In addition, the way of making this ferroelectric materials easier than superconductors. Although these ferroelectric materials have weaknesses such as the response time is not as fast as the photovoltaic sensors of HgCdTe, GaAs / AlGaAs and superconductors, but ferroelectric materials have advantage which do not require liquid nitrogen for cooling in ambient temperature, meaning they are easily made at laboratories of campus in Indonesia and world [1 – 5]. Ferro electricity is a symptom of spontaneous electrical polarization without the material receiving an electric from outside the material [1, 2, 10]. Ferroelectrics show that a group of dielectric materials can be polarized internally at a range of temperatures.

Polarization occurs within the dielectric as a result of the external electric field and symmetry on the crystallographic structure inside the unit cell. If the ferroelectric material is subjected to an electric field, certain atoms undergo a shift and generate an electric dipole moment. This dipole moment causes polarization [1, 11 – 12].

The most widely used of ferroelectric materials are $LiNbO_3$ [5] $LaTiO_3$ [4], $PbZrTiO_3$ [1], $PbZrO_3$, $BaxSr_1$-$xTiO_3$ (BST) [2], and BST doped metal oxide (BST derivative) [6]. A thin layer of LiNbO3, BST and its derivatives can be prepared by various methods such as sputtering [7, 10, 13-15], chemical solution deposition (CSD) [2 - 5, 16 - 20], pulsed laser deposition (PLD) 21], chemical vapor deposition (CVD) [22 - 23]. CSD method is relatively cheaper and easier compared to sputtering method, PLD, and CVD, then we in this research using CSD method [2 – 5].

Chemical Solution Deposition (CSD) method is one of the method of making thin film by using solution which is placed on the substrate, then rotated with certain speed with spin coating tool. Theoretical model and experiment for improving the quality of ferroelectric thin films by chemical solution deposition (CSD) and spin coating methods based on research done by previous researchers (24-26), were then modified by taking into account factors including surface tension, film viscosity, solution density, fluid flow rate, rotational speed, growth time, substrate form, and solvent evaporation process [27 – 30].

The perovskite structure of $LiNbO_3$, lithium ion (Li_2 $^{+)}$ is located at the tip of the cube ribs, the titanium ion (Nb_4 $^{+}$) is located in the diagonal of space and the oxygen ions is located in the diagonal of the cube plane. Addition of lanthanum into $LiNbO_3$ will

obtain a ferroelectric / pyroelectric / piezoelectric material resembling a p-type semiconductor (doping acceptor), since the Lanthanum (La_3^+) ion will occupy the position of lithium ion (Li_2^+) meaning that the structure has excess a positive ion (type- p) called hard dopant ions or dopant acceptor. Hard dopant ion can produce stronger ferroelectric materials, such as higher elastic conductivity, lower coercive field properties, higher mechanical quality factors and higher electrical current quality Dopant acceptors plays an important role in the formation of vacant space in the oxygen ion position (O_2^-) of the perovskite structure due to electrostatic processes, and causes Li ions to not easily leap into the oxygen ion space (O_2) due to blocked niobium ionic bonds. [31].

$LiNbO_3$ characteristic was closely related to the composition, its mineral structure, and its molecular shape. Thus, $LiNbO_3$ detection is crucial to understand the material characteristic deeper. There are several $LiNbO_3$ detection method such as X-ray powder diffraction (XRD), and also Fourier-transform infrared spectroscopy (FTIR).

X-ray powder diffraction (XRD) is a fast analysis method that mainly used for identificating crystal material phase and retrieving information about individual cell dimension. Analyzed material is homogenysis and composition. X-ray diffraction was based on constructive disturbance of monochromatic X-ray and crystal sample [32]. X-ray was emitted by catoda ray tube, filtered to creat monochromatic radiation, collimated for concentrating, and aimed at the sample [33 – 35]. Interaction between the X-ray and the sample create constructive interference (and the ray diffracted) if the condition meets the Bragg Law ($n\lambda = 2d \sin \theta$) yang menggunakan panjang gelombang 10 nm- 100 pm dan frekuensi : $3 \times 10^{16} – 3 \times 10^{18}$ Hz. The law explain the correlation between electromagnetic radiation wavelength with diffraction angle and grid distance on the cystal sample [36]. Diffracted X-ray is then detected, proceed and calculated. By scanning the sample with range of 2θ angles, all possible direction grid diffraction should be achieved due to the random orientation of the powder material. Conversion diffraction peak to distance-d enables the identification of mineral since each mineral has its unique set of distance-d. Usually, this is achieved by ratio of distance d and the standard benchmark pattern [37].

Fourier-transform infrared spectroscopy is a method used for retrieving infared spectrum in absorbtion or emission of solid-gas, solid or gas which was identified by vibration movement. Molecular vibration was unique for each molecul and usually called finger print vibration. Molecular vibration could be splitted into two groups; stretching vibration and bending vibration. A FTIR spectrometer could simultaniously collect high resolution spectrum data through wide spectrum range. In infrared spectroscopy, infrared spectrum was in the wavelength range from 0.75 to 1000 μm or wavenumber ranges from 1300 to 1 cm^{-1} with frequency of $3 \times 10^{12} – 3 \times 10^{14}$ Hz. From the application and instrumentation point of view, infrared spectrum divided into three radiation type which are near infrared (wavenumber of 12800-4000 cm^{-1}), mid infrared (wavenumber 4000-200 cm^{-1}), and far infrared (wavenumer of 200-10 cm^{-1}). This gives significant advantages over dispersive spectrometer which measure the intensity on the narrow range of wavelength over period of time. Name of Fourier-transform infrared spectroscopy comes from the fact that Fourire transformation (mathematical process) was needed to change raw data into the actual spectrum [38 – 40].

From the aforementioned explaination, studying atomic and molecular structure of $LiNbO_3$ are very important in order to studying the $LiNbO_3$ character itself. Analyzing X-ray Diffracton spectrum data usually with Rietveld model or General Structure Analysis System (GSAS). Both methods are based on reference as benchmark. The XRD data are compared with the reference data which then identified its characteristics [41]. ARIMA model could be used as alternative. ARIMA model does not need any reference pattern as benchmark. The research result showed that FTIR and XRD value on the heated $LiNbO_3$ thin films could be modelled well by ARIMA [42]. Thus, $LiNbO_3$ study through atomic and molecular structure could be studied through reflectant function which generated from XRD [43 – 53] and FTIR [54 – 63] value with ARIMA approach.

2. Research Objectives

1. Obtain $LiNbO_3$ ARIMA function from XRD and FTIR data,
2. Compared $LiNbO_3$ ARIMA function with XRD and FTIR data which doped by Lanthanum Oxide (0 %, 5 % dan 10 %)

3. Research Methodology

$LiNbO_3$ thin films manufacturing was conducted in two stages using chemical solution deposition method. In the first stage, substrate was prepared by cutting the p-type Si (100) with the size of 8 mm x 8 mm then cleaned by aqua and dried. In the next stage, the $LiNbO_3$ powder (precursor) was manufactured. There were three prepared prescursors i.e undoped precursor, 5% lanthanum doped precursor, and 10% lanthanum doped precursor. Precursors were obtained by mixing $LiCH_3COO$ powder, Nb_2O_5, and lanthanum oxide and then dissolved in 2.5 ml 2-methoxy methanol. The mixing process was conducted using ultrasonic of Branson 2210 for 90 minutes and then deposited on the substrate by using spin coating at speed of 3000 rpm, 2 times. The next step was annealing process using the furnace of VulcanTM3–130. The annealing process for each substrate was started from room temperature with the increasing rate of 1.7 ^oC/min to temperature of 550^oC and than held constantly for 8 hours. After that, cooled until room temperature [5].

FTIR spectrum characterization from $LiNbO_3$ thin film used FTIR tools type ABB MB 3000. In this research, FTIR spectrum used belongs to the mid infared radiaton category (wavenumber of 4000-500 cm^{-1}) with step of 16 cm^{-1}. XRD spectrum characterization used the XRD tools type GBC EMMA. In this research XRD spectrum used belongs to angle range of 100 to 800 with step of 0.02^0 [2 - 5].

ARIMA model exploration for FTIR and XRD data was done by Box and Jenkin procedure [64]. Initial step was done to identify the data was stationary or not in mean and in variance. Augmented Dickey-Fuller will be used. Augmented Dickey–Fuller test (ADF) tests the null hypothesis that a unit root is present in a time series sample. The alternative hypothesis is different depending on which version of the test is used, but is usually stationarity or trend-stationarity. It is an augmented version of the Dickey–Fuller test for a larger and more complicated set of time series models [64]. If it was not stationary in mean then differencing need to be done, and transformation needs to be

done if it was not stationary in variance. If the data was stationary, then ACF (Autocorrelation Function) plot and PACF (Partial Autocorrelation Function) plot were done to get possible assumption model [42]. Next step was to get estimated parameter model and to test the parameter to the models until significant model parameters were obtained. Selected model was then calculated its coefficient determination (R^2), Mean Absolut Percentage Error (MAPE), and plotted with the XRD data and FTIR to determine the accuracy of the model [42]. In this research, we used SPSS 15.0 for windows and Lenovo Computer 2 GB 64 Bit.

4. Result and Discussion

4.1. Raw Data of on $LiNbO_3$ FTIR value

Plot between infrared wavelength value as x-axis and absorbed, reflected, and transmitted percent of infrared as the y-axis on control Lanthanum Oxide (0%) doped Lithium Niobate was showed in Figure 1. Meanwhile in Figure 2 and Figure 3, it showed Plot between infrared wavelength value and absorbed, reflected, and transmitted percent of infrared Lanthanum Oxide (5%, 10%, respectively) doped Lithium Niobate. For ARIMA model, X-axis of FTIR data be changed to with integer number 1, 2, 3,.. which were consistent with wavelength value 1, 2, 3,.... Thus, Figure 1, 2, and 3 could be substitued with Figure 4, 5, and 6.

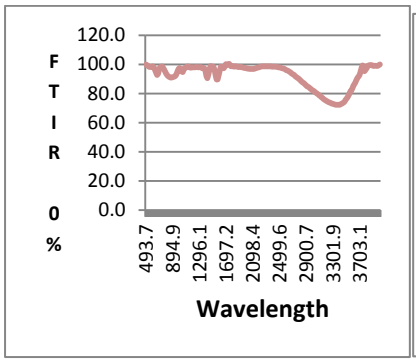

Figure 1. Plot FTIR data of Lanthanum Oxide (0%) Doped Lithium Niobate

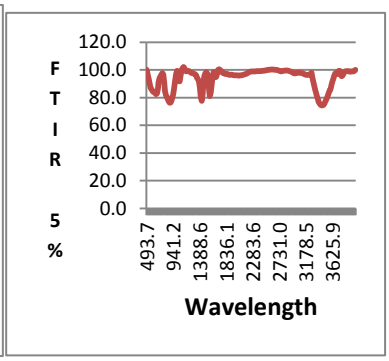

Figure 2. Plot FTIR data of Lanthanum Oxide (5%) Doped Lithium Niobate

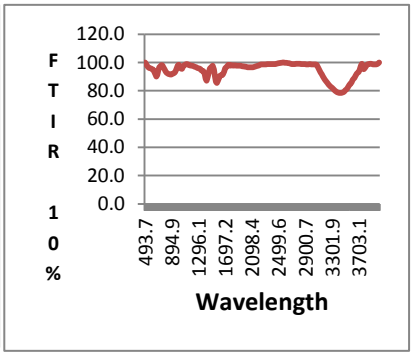

Figure 3. Plot FTIR data of Lanthanum Oxide (10%) Doped Lithium Niobate

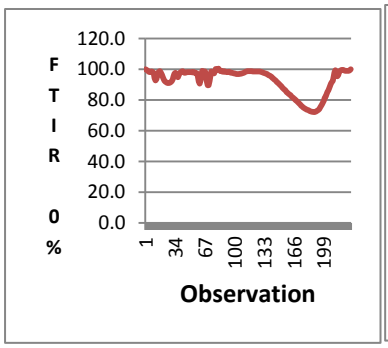

Figure 4. Plot FTIR data of Lanthanum Oxide (0%) Doped

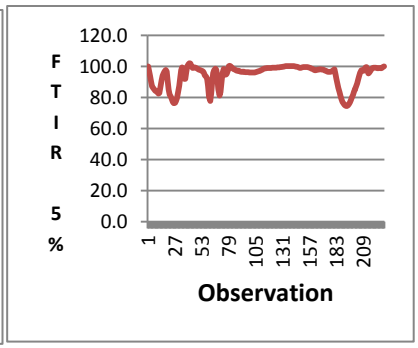

Figure 5. Plot FTIR data of Lanthanum Oxide (5%) Doped

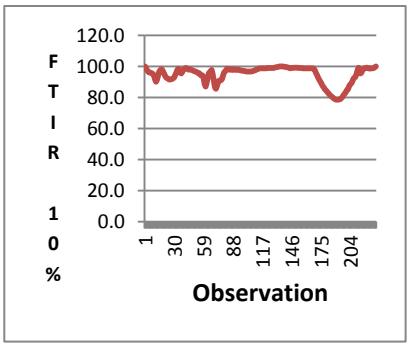

Figure 6. Plot FTIR data of Lanthanum Oxide (10%)

Lithium Niobate for ARIMA Model	Lithium Niobate for ARIMA Model	Doped Lithium Niobate for ARIMA Model

From Figure 4, 5, 6 and Augmented Dickey–Fuller test (ADF) with p-value < 0.0001, those FTIR data of Lanthanum Oxide (0 %, 5 %, 10 %) Doped Lithium Niobate are stationary in average. Non differensing of ARIMA model will be developed for FTIR data of Lanthanum Oxide (0 %, 5 %, 10 %) Doped Lithium Niobate.

4.2. ARIMA model on $LiNbO_3$ FTIR value

Partial Autocorrelation Function and Autocorrelation Function calculation of FTIR data of Lanthanum Oxide (0 %) doped Lithium Niobate was presented at Figure 7. ACF calculation tails off and PACF calculation cuts off at lag-3. From Figure 7, FTIR data suggest that the suitable model was ARIMA (3,0,0).

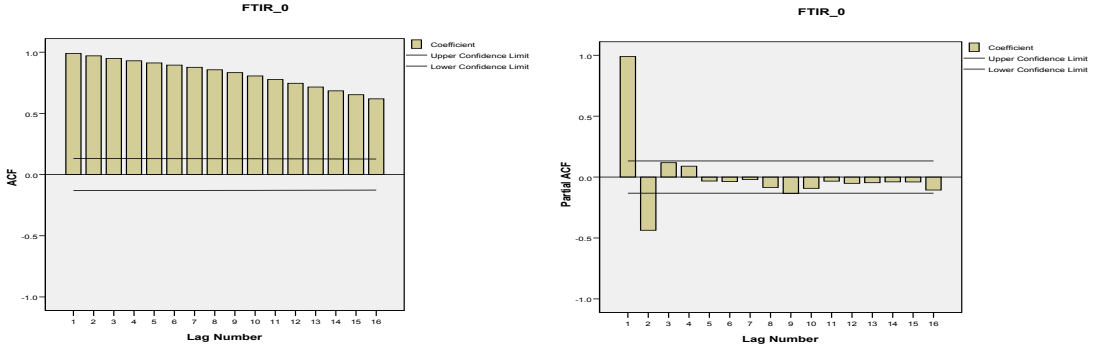

Figure 7. Plot ACF and PACF of FTIR data of Lanthanum Oxide (0%) Doped Lithium Niobate

ARIMA (3,0,0) parameters were estimated, those all parameters are significant with R^2 of 99 % and MAPE of 0,44 % which was presented in Table 1. Plot of actual data and the predicted data of ARIMA (3,0,0) on FTIR data of Lanthanum Oxide (0%) Doped Lithium Niobate is at Figure 8. Predicted data of ARIMA (3,0,0) on FTIR data of Lanthanum Oxide (0%) Doped Lithium Niobate followed actual data.

Table 1. ARIMA (3,0,0) model parameters for FTIR data of Lanthanum Oxide (0%) Doped Lithium Niobate

ARIMA (3,0,0)	Lag	Estimate	SE	t	Significant
	Constant	95.785	5.404	17.724	0.000
	Lag1	2.085	0.054	38.555	0.000
	Lag 2	-1.679	0.099	-16.985	0.000
	Lag 3	0.589	0.054	10.888	0.000

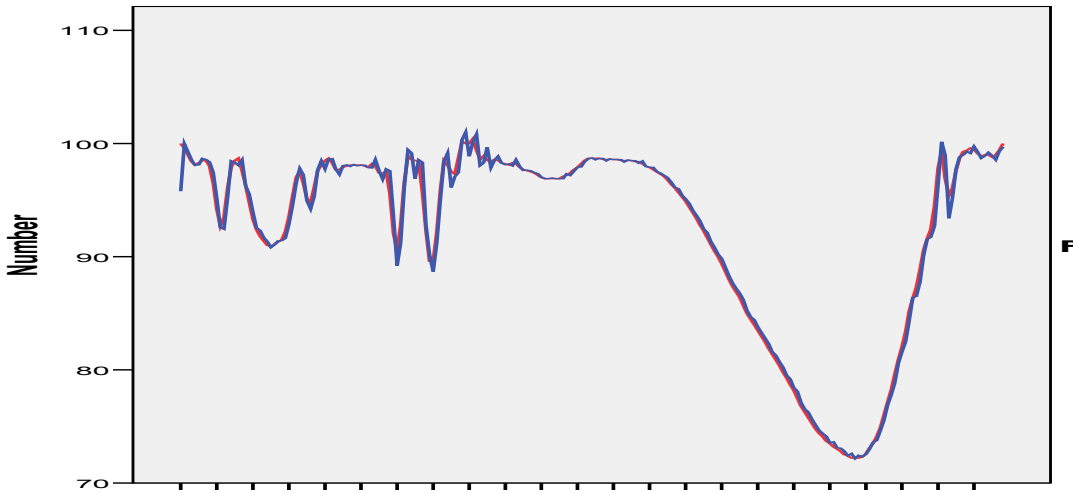

Figure 8. Plot of actual data and predicted pata of ARIMA (3,0,0) on FTIR data of Lanthanum Oxide (0%) Doped Lithium Niobate

From the process above, it could be concluded that FTIR data on Lanthanum Oxide (0%) Doped Lithium Niobate could be well predicted by ARIMA (3,0,0) with the equation model is (1):

$$y_t = 95.785 + 2.085\, y_{t-1} - 1.679\, y_{t-2} + 0.589\, y_{t-3}.$$

Partial Autocorrelation Function and Autocorrelation Function calculation of FTIR data of Lanthanum Oxide (5 %) doped Lithium Niobate is presented at Figure 9. ACF calculation tails off and PACF calculation cuts off at lag-3. From Figure 9, the suitable model for FTIR data of Lanthanum Oxide (5 %) doped Lithium Niobate was ARIMA (3,0,0).

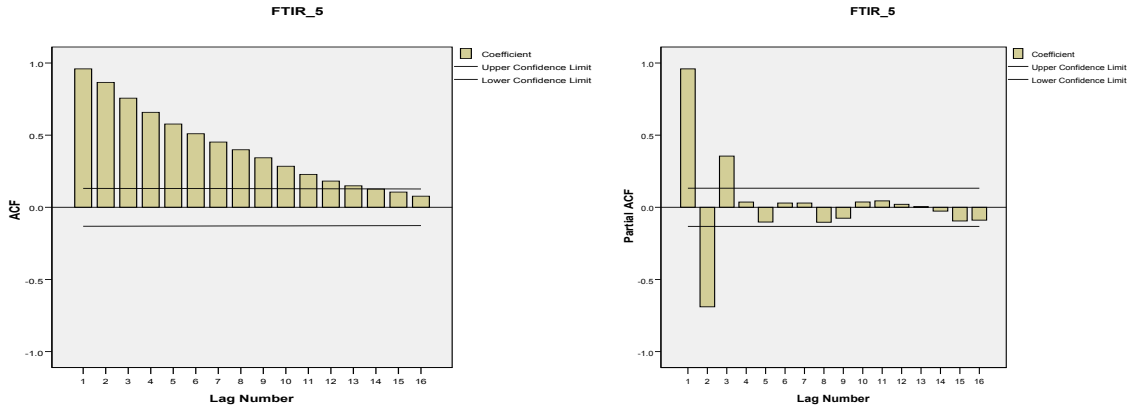

Figure 9. Plot ACF and PACF of FTIR data of Lanthanum Oxide (5%) Doped Lithium Niobate

ARIMA (3,0,0) parameters were estimated, those all parameters are significant with R^2 of 98 % and MAPE of 0.693 % which was presented in Table 2. Plot of actual data and the predicted data of ARIMA (3,0,0) on FTIR data of Lanthanum Oxide (5%) Doped

Lithium Niobate was presented at Figure 10. Predicted data ARIMA (3,0,0) of FTIR data of Lanthanum Oxide (5%) Doped Lithium Niobate followed followed actual data.

Table 2. ARIMA (3,0,0) parameters for FTIR data of Lanthanum Oxide (5%) Doped Lithium Niobate

ARIMA (3,0,0)	Lag	Estimate	SE	t	Significant
	Constant	94.924	2.354	40.321	0.000
	Lag1	2.168	0.053	41.233	0.000
	Lag 2	-1.806	0.095	-18.940	0.000
	Lag 3	0.612	0.052	11.679	0.000

So, it could be concluded that FTIR data of Lanthanum Oxide (5%) Doped Lithium Niobate could be well predicted by ARIMA (3,0,0) with the equation model is (2):

$$y_t = 94.924 + 2.168\, y_{t-1} - 1.806\, y_{t-2} + 0.612\, y_{t-3}.$$

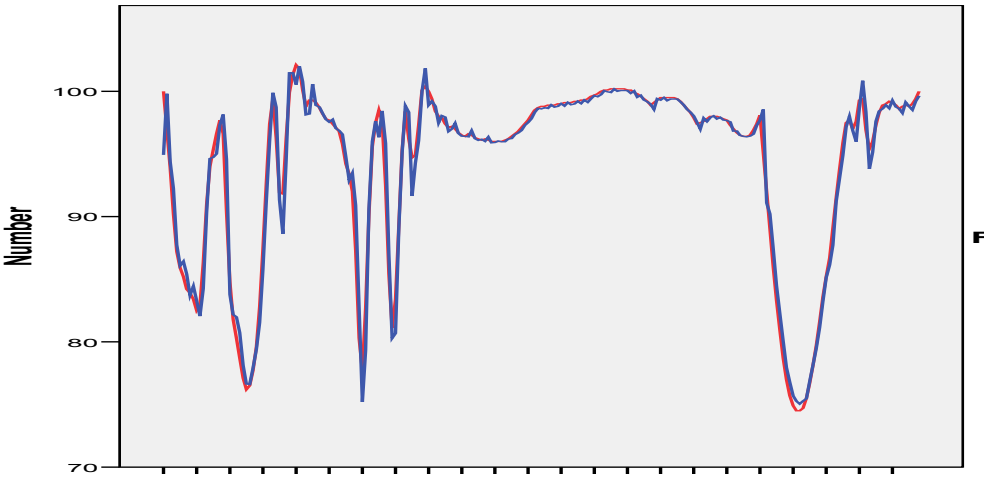

Figure 10. Plot of actual data and the predicted data of ARIMA (3,0,0) on FTIR data of Lanthanum Oxide (5%) Doped Lithium Niobate

Partial Autocorrelation Function and Autocorrelation Function calculation of FTIR data of Lanthanum Oxide (10 %) doped Lithium Niobate was presented by Figure 11. ACF calculation tails off and PACF calculation cuts off at lag-3. From Figure 11, the suitable model of FTIR of Lanthanum Oxide (10 %) doped Lithium Niobate was ARIMA (3,0,0).

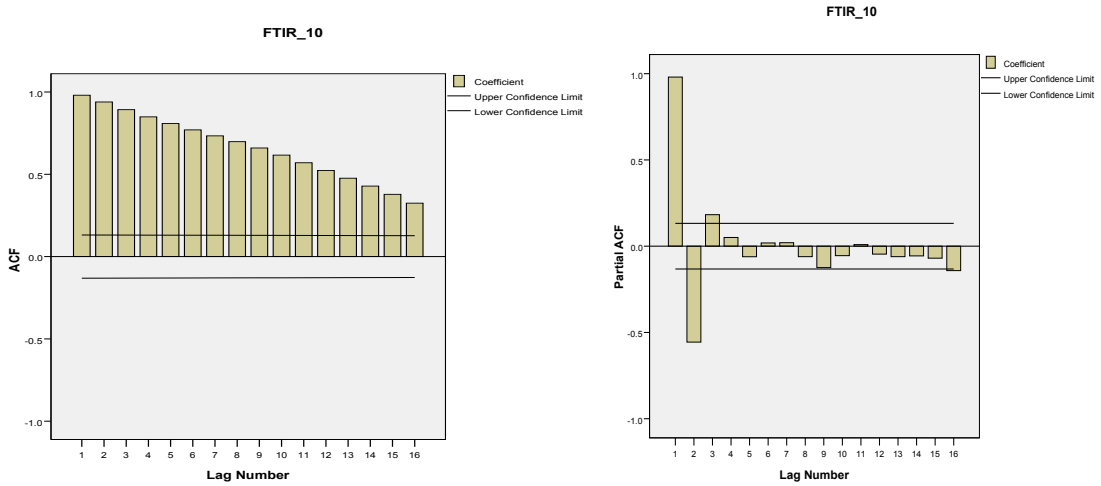

Figure 11. Plot ACF and PACF of FTIR data of Lanthanum Oxide (10%) Doped Lithium Niobate

ARIMA (3,0,0) model parameters were estimated and was presented at Table 3. From Table 3 showed those ARIMA (3,0,0) model parameters were siginificant.

Table 3. ARIMA (3,0,0) model parameters for FTIR data of Lanthanum Oxide (10 %) Doped Lithium Niobate

ARIMA (3,0,0)	Lag	Estimate	SE	t	Significant
	Constant	96.031	2.798	44.320	0.000
	Lag1	2.124	0.054	39.167	0.000
	Lag 2	-1.716	0.099	-17.257	0.000
	Lag 3	0.581	0.054	10.717	0.000

ARIMA (3,0,0) model for FTIR data of Lanthanum Oxide (10 %) Doped Lithium Niobate has Coefficient Determination of 99 % and MAPE of 0.403 %. Predicted data of ARIMA (3,0,0) on FTIR data of Lanthanum Oxide (10%) Doped Lithium Niobate followed actual data (Figure 12).

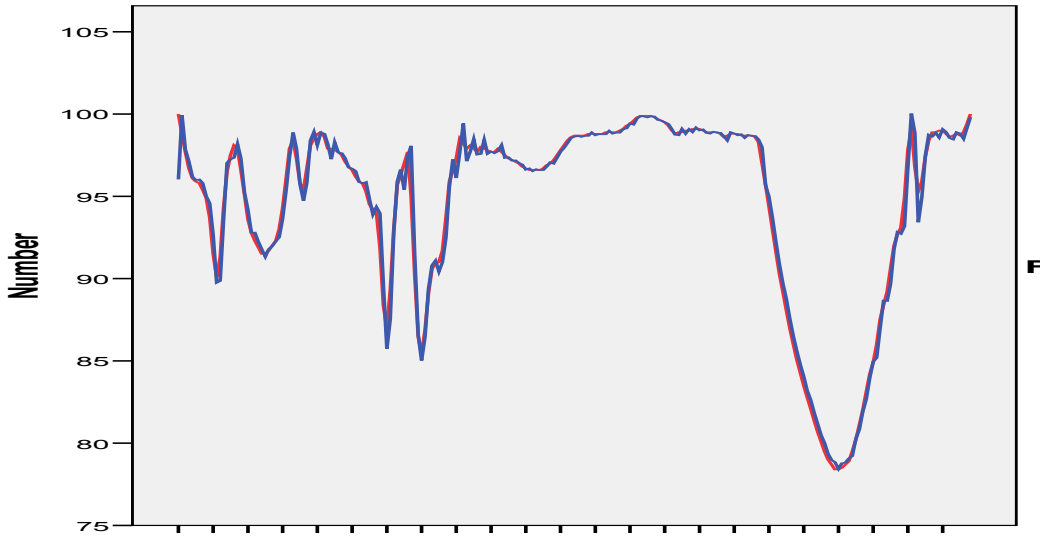

Figure 12. Plot of actual data and the predicted data of ARIMA (3,0,0) on FTIR data of Lanthanum Oxide (10%) Doped Lithium Niobate

So, it could be concluded that FTIR data on Lanthanum Oxide (10%) Doped Lithium Niobate could be well predicted by ARIMA (3,0,0) with the equation model (3):

$$y_t = 96{,}031 + 2.124\, y_{t-1} - 1.716 y_{t-2} + 0.581\, y_{t-3}$$

4.3. Raw Data of on $LiNbO_3$ XRD value

Plot between angle value as x-axis and and reflected intensity value (XRD) as y-axis on Lanthanum Oxide (0%, 5%, 10%) doped Lithium Niobate (Figure 13, 14, 15). For ARIMA model, X-axis of XRD data be changed by integer number 1, 2, 3,.. which were consistent with wavelength value 1, 2, 3,.... Thus, Figure 13, 14, and 15 will be substitued with Figure 16, 17, and 18.

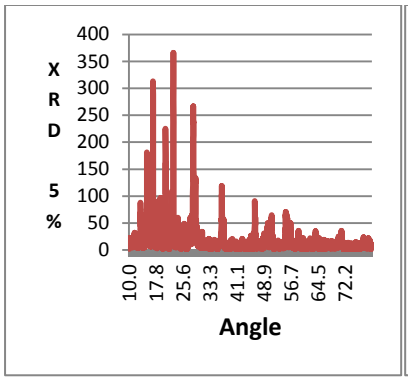

Figure 13. Plot XRD data of Lanthanum Oxide (0%) Doped Lithium Niobate

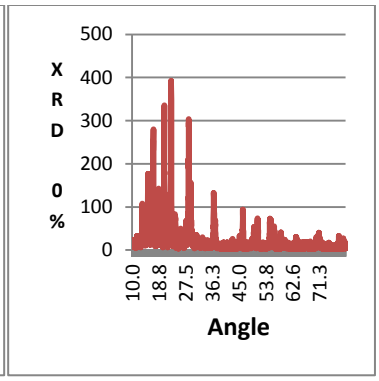

Figure 14. Plot XRD data of Lanthanum Oxide (5%) Doped Lithium Niobate

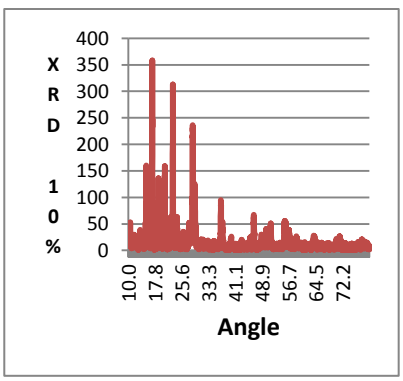

Figure 15. Plot XR data of Lanthanum Oxide (10%) Doped Lithium Niobate

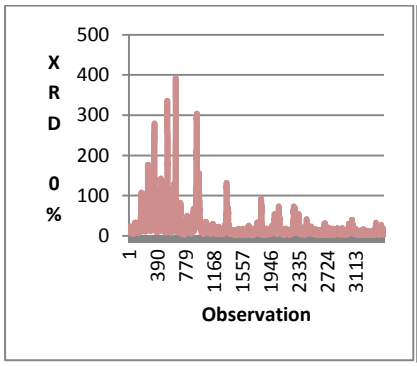

Figure 16. Plot XRD data of Lanthanum Oxide (0%) Doped Lithium Niobate for ARIMA Model

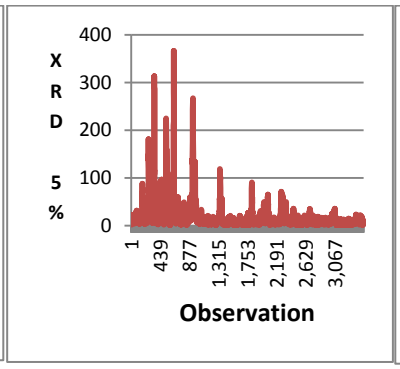

Figure 17. Plot XRD data of Lanthanum Oxide (5%) Doped Lithium Niobate for ARIMA Model

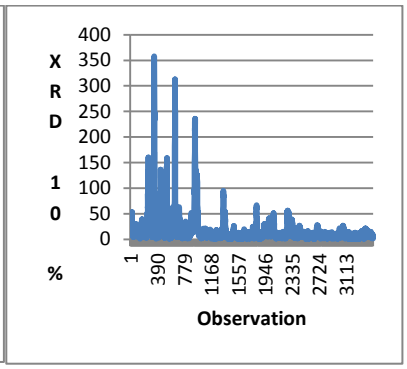

Figure 18. Plot XRD data of Lanthanum Oxide (10%) Doped Lithium Niobate for ARIMA Model

From Figure 16, 17, 18 and Augmented Dickey–Fuller test (ADF) with p-value < 0.0001, those XRD data of Lanthanum Oxide (0 %, 5 %, 10 %) Doped Lithium Niobate were stationary in average. Non differensing of ARIMA model will be developed for XRD data of Lanthanum Oxide (0 %, 5 %, 10 %) Doped Lithium Niobate.

4.4. ARIMA model on $LiNbO_3$ XRD value

Partial Autocorrelation Function and Autocorrelation Function calculation of XRD data of Lanthanum Oxide (0 %) doped Lithium Niobate was presented by Figure 19. ACF calculation tails off and PACF calculation cuts off at lag-5, that means nondifferencing ARIMA model was AR(5) and MA (0). Thus, From Figure 19, the model for XRD data of Lanthanum Oxide (0 %) Doped Lithium Niobate was ARIMA (5,0,0).

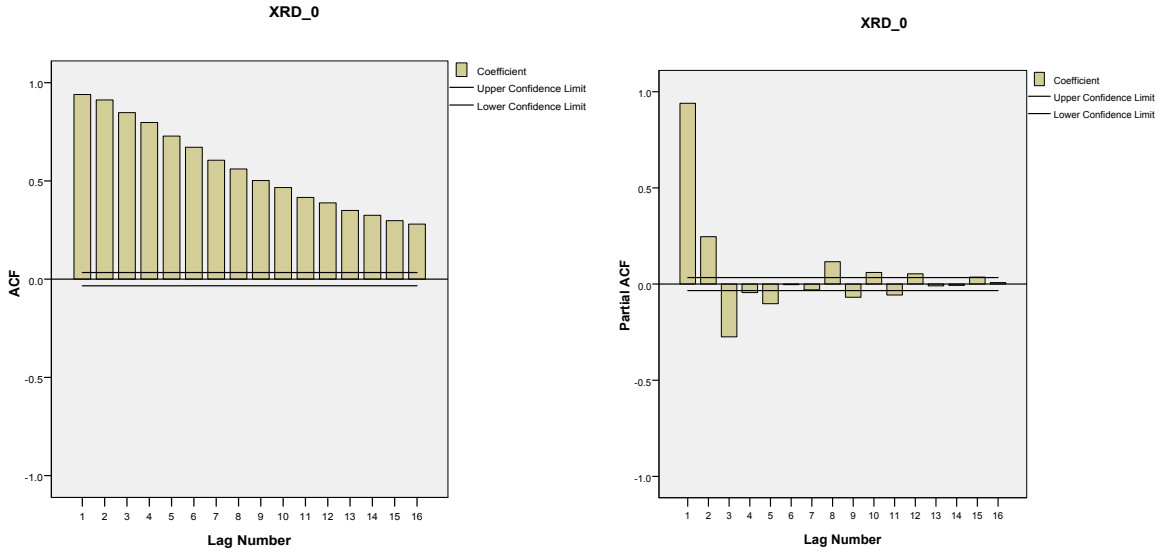

Figure 19. Plot ACF and PACF of XRD data of Lanthanum Oxide (0%) Doped Lithium Niobate

ARIMA (5,0,0) model parameters were estimated. Hopefully those all parameters of ARIMA (5,0,0) model were significants with R^2 of 90 % which be presented in Table 4. Table 4 showed that not All ARIMA (5,0,0) model parameters were significant, they are only four parameters of model were significant. Thus, XRD data of Lanthanum Oxide (0%) Doped Lithium Niobate better to be modelled by ARIMA (4,0,0) model (Tabel 5). All ARIMA (4,0,0) parameters were significant, with R^2 of 90 % and MAPE of 42,972 %. Figure 20 showed that predicted data of ARIMA (4,0,0) model on XRD data of Lanthanum Oxide (0%) Doped Lithium Niobate followed actual data (Figure 20).

Table 4. ARIMA (5,0,0) model parameters for XRD data of Lanthanum Oxide (0%) Doped Lithium Niobate

ARIMA (5,0,0)	Lag	Estimate	SE	t	Significant
	Constant	20.723	-2.498	8.295	0.000
	Lag1	0.759	0.017	45.104	0.000
	Lag 2	0.436	0.021	20.667	0.000
	Lag 3	-0.193	0.022	-8.700	0.000
	Lag 4	0.034	0.021	1.589	0.112
	Lag 5	-0.102	0.017	-6.074	0.000

Table 5. ARIMA (4,0,0) model parameters for XRD data of Lanthanum Oxide (0%) Doped Lithium Niobate

ARIMA (4,0,0)	Lag	Estimate	SE	t	Significant
	Constant	20.707	2.764	7.492	0.000
	Lag1	0.763	0.017	45.188	0.000
	Lag 2	0.461	0.021	22.064	0.000
	Lag 3	-0.240	0.021	-11.497	0.000
	Lag 4	-0.044	0.017	-2.631	0.009

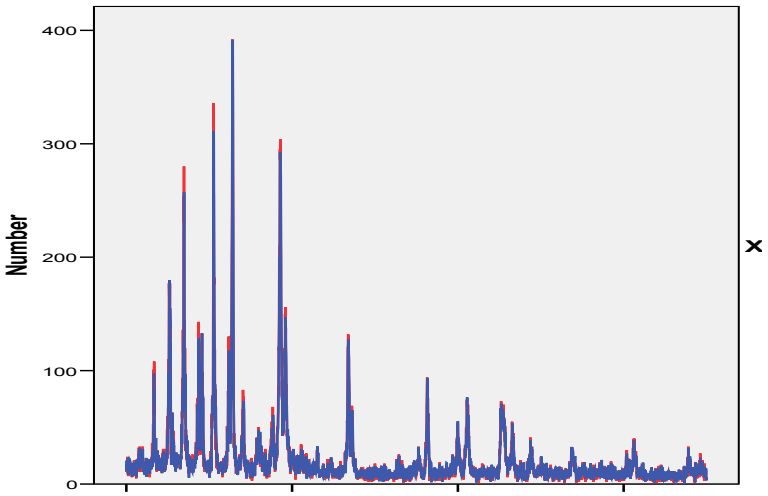

Figure 20. Plot of actual and the predicted data of ARIMA (4,0,0) on XRD data of Lanthanum Oxide (0%) Doped Lithium Niobate

From the process above, it could be concluded that XRD data on Lanthanum Oxide (0%) Doped Lithium Niobate could be well predicted by ARIMA (4,0,0) with the equation model (4):

$$y_t = 20.707 + 0.763\, y_{t-1} + 0.461\, y_{t-2} - 0.240\, y_{t-3} - 0.044\, y_{t-4}$$

Partial Autocorrelation Function and Autocorrelation Function calculation of XRD data of Lanthanum Oxide (5 %) doped Lithium Niobate were presented at Figure 21. ACF calculation tails off and PACF calculation cuts off at lag-4, that means nondifferencing ARIMA model were AR(4) and MA (0). Thus, From Figure 21, the model for XRD data of Lanthanum Oxide (5 %) Doped Lithium Niobate was ARIMA (4,0,0).

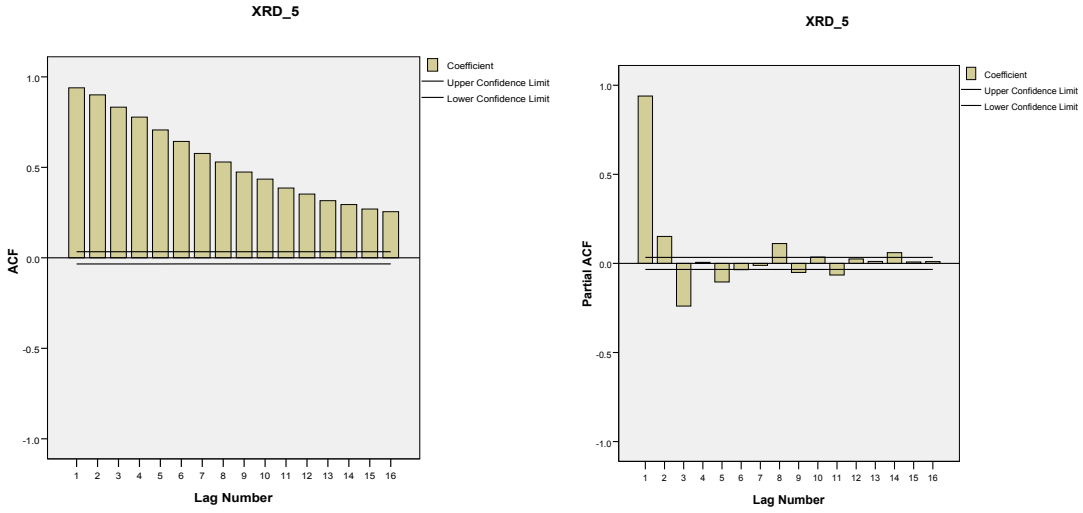

Figure 21. Plot ACF and PACF of XRD data of Lanthanum Oxide (5%) Doped Lithium Niobate

ARIMA (4,0,0) model parameters were estimated. Hopefully those all parameters of ARIMA (4,0,0) model were significants with R^2 of 89 % which be presented in Table 6. Table 6 showed that not All ARIMA (4,0,0) model parameters were significant, they are only three parameters of model were significant. Thus, XRD data of Lanthanum Oxide (5%) Doped Lithium Niobate better to be modelled by ARIMA (3,0,0) model (Tabel 7). All ARIMA (3,0,0) model parameters were significant which R^2 of 89 % and MAPE of 51.237 % . Figure 22 showed that predicted data of ARIMA (3,0,0) model on XRD data of Lanthanum Oxide (5%) Doped Lithium Niobate followed actual data (Figure 22).

Table 6. ARIMA (4,0,0) model parameters for XRD data of Lanthanum Oxide (5%) Doped Lithium Niobate

ARIMA (4,0,0)	Lag	Estimate	SE	t	Significant
	Constant	17.277	2.339	7.385	0.000
	Lag1	0.835	0.017	49.351	0.000
	Lag 2	0.340	0.022	15.725	0.000

	Lag 3	-0.244	0.022	-11.293	0.000
	Lag 4	0.006	0.017	0.350	0.725

© 2018 IJSRSET | Volume 4 | Issue 4 | Print ISSN: 2395-1990 | Online ISSN : 2394-4099
Themed Section : Engineering and Technology

Table 7. ARIMA (4,0,0) model parameters for XRD data of Lanthanum Oxide (5%) Doped Lithium Niobate

ARIMA (3,0,0)	Lag	Estimate	SE	t	Significant
	Constant	17.277	2.326	7.429	0.000
	Lag1	0.833	0.016	50.751	0.000
	Lag 2	0.342	0.021	16.419	0.000
	Lag 3	-0.239	0.016	-14.584	0.000

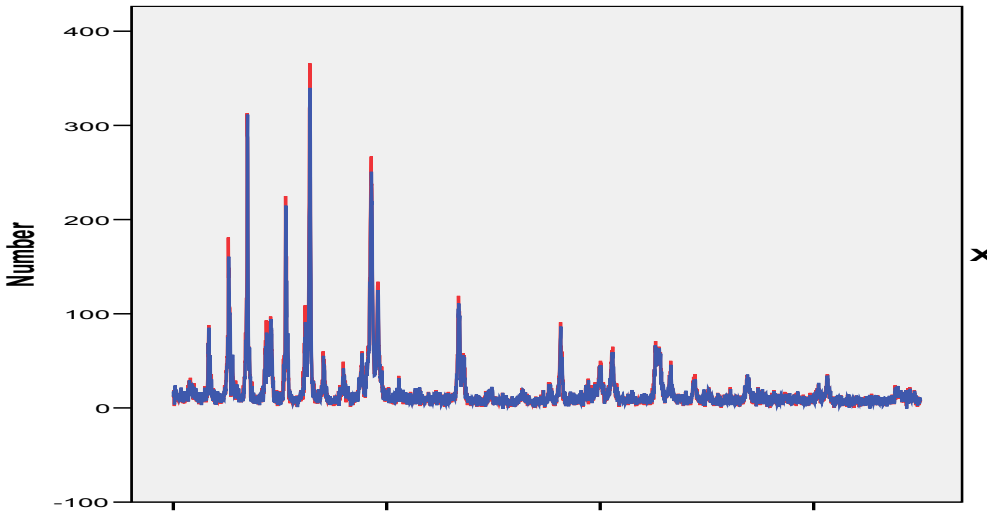

Figure 22. Plot of actual and the predicted data of ARIMA (3,0,0) on XRD data of Lanthanum Oxide (5%) Doped Lithium Niobate

From the process above, it could be concluded that XRD data on Lanthanum Oxide (5%) Doped Lithium Niobate could be well predicted by ARIMA (3,0,0) with the equation model is (5):

$$y_t = 17{,}277 + 0{,}833\, y_{t-1} + 0{,}342\, y_{t-2} - 0{,}239\, y_{t-3}$$

Partial Autocorrelation Function and Autocorrelation Function calculation of XRD data of Lanthanum Oxide (10 %) doped Lithium Niobate were presented at Figure 23. ACF calculation tails off and PACF calculation cuts off at lag-5, that means nondifferencing ARIMA model were AR(5) and MA (0). Thus, From Figure 23, the model for XRD data of Lanthanum Oxide (10 %) Doped Lithium Niobate was ARIMA (5,0,0).

© 2018 IJSRSET | Volume 4 | Issue 4 | Print ISSN: 2395-1990 | Online ISSN : 2394-4099
Themed Section : Engineering and Technology

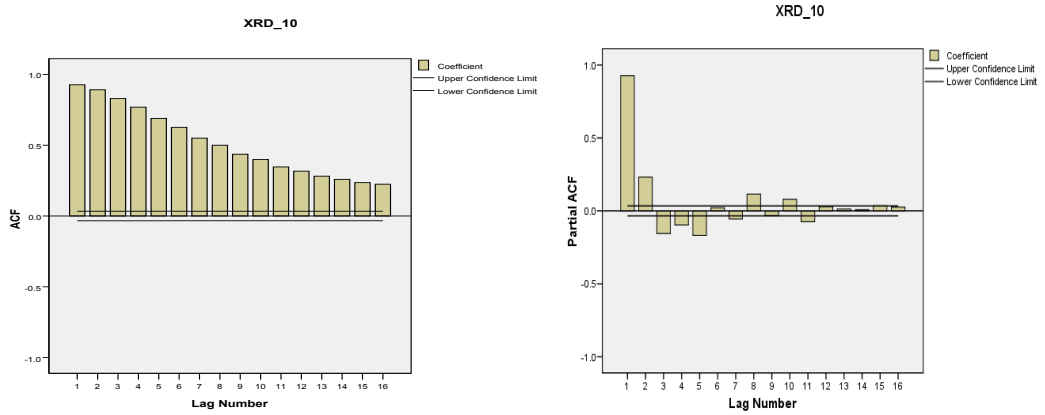

Figure 23. Plot ACF and PACF of XRD data of Lanthanum Oxide (10%) Doped Lithium Niobate

ARIMA (5,0,0) model parameters were estimated, but they were only three parameters of model were significant. Thus, XRD data of Lanthanum Oxide (10 %) Doped Lithium Niobate better to be modelled by ARIMA (3,0,0) model (Tabel 8). All ARIMA (3,0,0) model parameters were significant which R^2 of 87 % and MAPE of 50,882 % (Table 9). Figure 22 showed that predicted data of ARIMA (3,0,0) model on XRD data of Lanthanum Oxide (5%) Doped Lithium Niobate followed actual data (Figure 24).

Table 8. ARIMA (5,0,0) model parameters for XRD data of Lanthanum Oxide (10%) Doped Lithium Niobate

ARIMA (5,0,0)	Lag	Estimate	SE	t	Significant
	Constant	15,173	1,721	8,818	0,000
	Lag1	0.717	0.017	42.980	0.000
	Lag 2	0.361	0.021	17.517	0.000
	Lag 3	-0.020	0.021	-0.924	0.355
	Lag 4	0.027	0.021	1.314	0.189
	Lag 5	-0.168	0.017	-10.087	0.000

Table 9. ARIMA (3,0,0) model parameters for XRD data of Lanthanum Oxide (10%) Doped Lithium Niobate

ARIMA (3,0,0)	Lag	Estimate	SE	t	Significant
	Constant	15.151	2.237	6.772	0.000
	Lag1	0.748	0.017	44.762	0.000
	Lag 2	0.342	0.020	16.986	0.000
	Lag 3	-0.155	0.017	-9.279	0.000

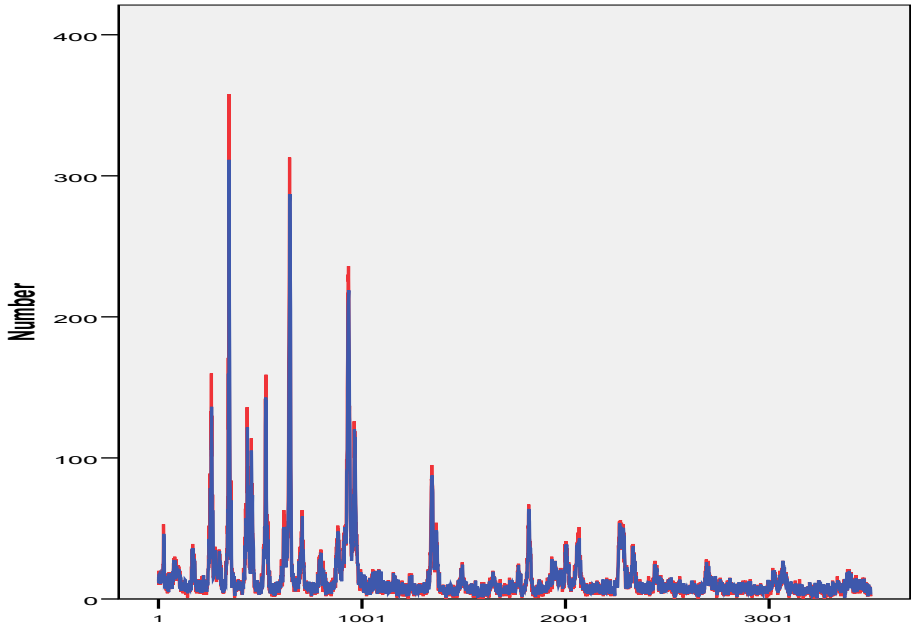

Figure 24. Plot of actual and the predicted data of ARIMA (3,0,0) on XRD data of Lanthanum Oxide (10%) Doped Lithium Niobate

From the process above, it could be concluded that XRD data on Lanthanum Oxide (10 %) Doped Lithium Niobate could be well predicted by ARIMA (3,0,0) with the equation model is (6):

$$y_t = 15{,}151 + 0{,}748\, y_{t-1} + 0{,}342\, y_{t-2} - 0{,}155\, y_{t-3}$$

4.5. Effect of Lanthanum Oxide to FTIR, and XRD value of Lithium Niobate

Lithium Niobate was doped by lanthanum oxide with three concentrations such as 0%, 5% and 10 %. The effect of Lanthanum Oxide were measured by FTIR and XRD value. The mean of FTIR value of Lanthanum Oxide (0%, 5%, 10 %) doped Lithium Niobate are 92.4538, 94.2459, 94,7088, respectively.

To compare effect of Lanthanum Oxide doped to of Lithium Niobate was used by comparing mean of FTIR values of Lanthanum Oxide (0%, control) doped Lithium Niobate control versus Lanthanum Oxide (5%) doped Lithium Niobate and Lanthanum Oxide (0%, control) doped Lithium Niobate control versus Lanthanum Oxide (10%) doped Lithium Niobate, with null hypothesis : mean of FTIR value of Lanthanum Oxide (0%, control) doped Lithium Niobate same with FTIR value of Lanthanum Oxide (5%) doped Lithium Niobate and mean of FTIR value of Lanthanum Oxide (0%, control) doped Lithium Niobate same with FTIR value of Lanthanum Oxide (10%) doped Lithium Niobate.

By using t-test with assumption independent population and equal variance between Lanthanum Oxide (0%, control) doped Lithium Niobate and Lanthanum Oxide (5 %) doped Lithium Niobate, t-value of mean of FTIR values of Lanthanum Oxide (0%, control) doped Lithium Niobate control versus Lanthanum Oxide (5%) doped Lithium

Niobate is 2.447 (456 degrees of freedom) with p-value =0.014. We can say there is difference of mean of FTIR value between Lanthanum Oxide (0%, control) doped Lithium Niobate and Lanthanum Oxide (5 %) doped Lithium Niobate. Lithium Niobate was doped by Lanthanum Oxide 5% can make increasing of FTIR value from 92.4538 to 94.2459, significantly (Table 10). Also, with the same assumption, t-value of mean of FTIR values of Lanthanum Oxide (0%, control) doped Lithium Niobate control versus Lanthanum Oxide (10 %) doped Lithium Niobate was 3.382 (456 degrees of freedom)with p-value =0.001. We can say there is difference of mean of FTIR value between Lanthanum Oxide (0%, control) doped Lithium Niobate and Lanthanum Oxide (10 %) doped Lithium Niobate. Lithium Niobate was doped by Lanthanum Oxide 10 % can make increasing of FTIR value from 92.4538 to 94,7088, significantly (Table 11). Increasing of FTIR value from 92.4538, 94.2459, 94,7088 that indicated adding Lanthanum Oxide to Lithium Niobate ($LiNbO_3$) can increase absorbing of $LiNbO_3$. That process caused by increasing of activities energy structure molecul of $LiNbO_3$ to infrared spectral energy [5].

Table 10. Group Statistics and Samples test of FTIR values of Lanthanum Oxide (0%, control) doped Lithium Niobate and Lanthanum Oxide (5 %) doped Lithium Niobate

Group	N	Mean of FTIR	Assumption	t-value	p-value
Lanthanum Oxide (0%, control) doped Lithium Niobate	229	92,4538	Equal variance	2,447	0.014
Lanthanum Oxide (5 %) doped Lithium Niobate	229	94,2486			

Table 11. Group Statistics and Samples test of FTIR values of Lanthanum Oxide (0%, control) doped Lithium Niobate and Lanthanum Oxide (10 %) doped Lithium Niobate

Group	N	Mean of FTIR	Assumption	t-value	p-value
Lanthanum Oxide (0%, control) doped Lithium Niobate	229	92,4538	Equal variance	3.382	0.001
Lanthanum Oxide (10 %) doped Lithium Niobate	229	94,7088			

The mean of XRD value of Lanthanum Oxide (0%, 5%, 10 %) doped Lithium Niobate were 20.8061, 17.3256, 15.2168, respectively.

Table 12. Group Statistics and Samples test of XRD values of Lanthanum Oxide (0%, control) doped Lithium Niobate and Lanthanum Oxide (5 %) doped Lithium Niobate

Group	N	Mean of XRD	Assumption	t-value	p-value
Lanthanum Oxide (0%, control) doped Lithium Niobate	3501	20.8061	Equal variance	5.007	0.000
Lanthanum Oxide (5 %) doped Lithium Niobate	3501	17.3256			

Table 13. Group Statistics and Samples test of XRD values of Lanthanum Oxide (0%, control) doped Lithium Niobate and Lanthanum Oxide (10 %) doped Lithium Niobate

Group	N	Mean of XRD	Assumption	t-value	p-value
Lanthanum Oxide (0%, control) doped Lithium Niobate	3501	20,8061	Equal variance	8.406	0.000
Lanthanum Oxide (10 %) doped Lithium Niobate	3501	15.2168			

By using t-test with assumption independent population and equal variance between Lanthanum Oxide (0%, control) doped Lithium Niobate and Lanthanum Oxide (5 %) doped Lithium Niobate, comparing mean of XRD values of Lanthanum Oxide (0%, control) doped Lithium Niobate control versus Lanthanum Oxide (5%) doped Lithium Niobate had t-value of 5.007 (7000 degrees of freedom) with p-value =0.000. We can say there is difference of mean of XRD value between Lanthanum Oxide (0%, control) doped Lithium Niobate and Lanthanum Oxide (5 %) doped Lithium Niobate. Lithium Niobate was doped by Lanthanum Oxide 5% can make decreasing of XRD value from 20.8061 to 17.3256, significantly. Also, with the same assumption, t-value of mean of XRD value of Lanthanum Oxide (0%, control) doped Lithium Niobate and Lanthanum Oxide (10 %) doped Lithium Niobate was 8.406 (7000 degrees of freedom) with p-value =0.000. We

can say there is difference of mean of XRD value between Lanthanum Oxide (0%, control) doped Lithium Niobate and Lanthanum Oxide (10 %) doped Lithium Niobate. Lithium Niobate was doped by Lanthanum Oxide 10 % can make decreasing of XRD value from 20.8061 to 15.2168, significantly. Decreasing of XRD value from 20.8061, 17.3256, 15.2168 that indicated parameter hints of $LiNbO_3$ decreases which influenced by the radius of its contituuent ions. Ionic radii of Li^+, Nb^{5+} and La^{3+} are 0.90 Å, 0.78 Å and 1.172 Å, respectively. It can be seen that the Ionic radius of La^{3+} is closer to Ionic radius of Li^+ so that La^{3+} can occupy the positions of Li^+ in the crystal structure. The difference of ionic radii between the dopant and the replaced ion affects the formation of spinel phase, which leads to crystal size decreasing to its existence of dopant's cations in the structure of $LiNbO_3$ [5].

5. Conclusion

- ARIMA model can be used to model for FTIR and XRD values of Lanthanum Oxide (0%, 5 %, 10 %) doped Lithium Niobate and Lanthanum Oxide with high accuracy, since it has R^2 greater than 80 % and predicted values from ARIMA model followed behaviour actual data.
- FTIR data on Lanthanum Oxide (0%) Doped Lithium Niobate could be well predicted by ARIMA (3,0,0) with the equation model :
$$y_t = 95{,}785 + 2{,}085\, y_{t-1} - 1.679\, y_{t-2} + 0{,}589\, y_{t-3}.$$
- FTIR data on Lanthanum Oxide (5%) Doped Lithium Niobate could be well predicted by ARIMA (3,0,0) with the equation model :
$$y_t = 94{,}924 + 2{,}168\, y_{t-1} - 1{,}806\, y_{t-2} + 0{,}612\, y_{t-3}.$$
- FTIR data on Lanthanum Oxide (10%) Doped Lithium Niobate could be well predicted by ARIMA (3,0,0) with the equation model :
$$y_t = 96{,}031 + 2{,}124\, y_{t-1} - 1{,}716 y_{t-2} + 0{,}581\, y_{t-3}$$
- XRD data on Lanthanum Oxide (0%) Doped Lithium Niobate could be well predicted by ARIMA (4,0,0) with the equation model :
$$y_t = 20{,}707 + 0{,}763\, y_{t-1} + 0{,}461\, y_{t-2} - 0{,}240\, y_{t-3} - 0{,}044\, y_{t-4}$$
- XRD data on Lanthanum Oxide (5%) Doped Lithium Niobate could be well predicted by ARIMA (3,0,0) with the equation model :
$$y_t = 17{,}277 + 0{,}833\, y_{t-1} + 0{,}342\, y_{t-2} - 0{,}239\, y_{t-3}$$
XRD data on Lanthanum Oxide (10 %) Doped Lithium Niobate could be well predicted by ARIMA (3,0,0) with the equation model :
$$y_t = 15{,}151 + 0{,}748\, y_{t-1} + 0{,}342\, y_{t-2} - 0{,}155\, y_{t-3}$$
- ARIMA model l for FTIR data is more accurate than ARIMA model for XRD data, since R^2 of ARIMA model of FTIR data is greater than R^2 of ARIMA model of XRD data and MAPE of of ARIMA model of FTIR data is lower than MAPE of of ARIMA model of XRD data.
- Lanthanum oxide doped to lithium niobate Increasing of FTIR value that indicated adding Lanthanum Oxide to Lithium Niobate ($LiNbO_3$) can increase absorbing of $LiNbO_3$ and has lowered the XRD 2168 that indicated parameter hints of $LiNbO_3$ decreases which influenced by the radius of its contituuent ions.

6. Acknowledgement

This work was supported by Penelitian Unggulan Divisi (PUD), Ministry of Research, Technology, and Higher Education; Republic of Indonesia No. 011/SP2H/LT/DRPM/ IV/2017. Thanks also to the Indonesian Government who had given the chance for the authors to conduct this research.

Refferences

1. Irzaman, Y. Darvina, A. Fuad, P. Arifin, M. Budiman, and M. Barmawi. Physical and Pyroelectric Properties of Tantalum Oxide Doped Lead Zirconium Titanate [Pb0.9950(Zr0.525Ti0.465Ta0.010)O_3] Thin Films and Its Application for IR Sensor. Physica Status Solidi (a), Germany**, 199** (3), 416 – 424, 2003.
2. Irzaman, H. Syafutra, E. Rancasa, A. Wahidin Nuayi, Tb. Gamma Nur Rahman, N. Aisyah Nuzulia, I. Supu, Sugianto, F. Tumimomor, Surianty, O. Muzikarno, and Masrur. The Effect of BaSr Ratio on Electrical and Optical Properties of $Ba_xSr_{(1-x)}TiO_3$ (x = 0.25; 0.35; 0.45; 0.55) Thin Film Semiconductor. Ferroelectrics. **445** (1) : 4-17, 2013.
3. Irzaman, Ridwan Siskandar, Aminullah, Irmansyah, and Husin Alatas. Characterization of $Ba_{0,55}Sr_{0.45}TiO_3$ Films As Light And Temperature Sensors And Its Implementation on Automatic Drying System Model. Integrated Ferroelectrics. **168** (1), 130-150, 2016.
4. Irzaman, Y. Pebriyanto, E. Rosidah Apipah, I. Noor, A. Alkadri. Characterization of Optical and Structural of Lanthanum Doped $LiTaO_3$ Thin Films. Integrated Ferroelectrics. **167**(1), 137-145, 2015.
5. Irzaman, Henni Sitompul, Masitoh, Mohammad Misbakhusshudur and Mursyidah. Optical and Structural Properties of Lanthanum Doped Lithium Niobate Thin Films. Ferroelectrics. **502** (1), 9-18, 2016.
6. Wu, N.J, Y.S. Chen, S. Dorderic, A. Ignatiev. Pyroelectric IR Sensor Based on Oxide Heterostructures on Si (100) and $LaAlO_3$ (100) Substrates. Proceeding Third International Conference on Thin Film Physiscs and Applications. SPIE Vol. **3175**, page 256 – 261.
7. Lee, B.T, W.D. Kim, K.H. Lee, H.J. Lim, C.S. Kang, H. Hideki. Electrical Properties of Sputtered BST Thin Films Prepared by Two Step Deposition Method. Journal of electronic Materials. **28** (4), L9 – L12, 1999.
8. Itskovsky. M.A. Kinetics of Ferroelectric Phase Transition : Nonlinear Pyroelectric Effect and Ferroelectric Solar Cell. Jpn. J. Appl. Phys. **38** (8), 4812 – 4817, 1999.
9. Whitaker, T. Focal Plane Arrays Fabricated from Compound Semiconductor Materials are at The Heart of Many Infrared Imaging Systems and Nigth Vision Cameras. Compound Semiconductor Spring II, **4** (4), 17 –23, 1998.
10. Izuha, M., and K. Abe. Electrical Properties and Microstructure of Pt/BST/$SrRuO_3$ Capacitors. Appl. Phys. Lett. **70** (11), 1405 – 1407, 1997.
11. Miles. R. W. Photovoltaic solar cells; Choice of materials and production methods. Science direct, Vacuum, **80**, 1090-1097, 2006.
12. Galiana, B., I. R. Stole, M.Baudrit, I. Garcia and C. Algora. A comparative study of BSFlayers for GaAs-based single-junction or multijunction concentrator solar cells. Institute of physics publishing, Semicond, Sci. Technol, **21**, 1387-1392, 2006.

13. Shin, J.C., J. Park, C.S. Hwang and H.J. Kim. *Dielectric and Electrical Properties of Sputter Grown BST Thin Films.* J. Appl. Phys. **86** (1), 506 – 513, 1999.
14. Kawakubo, T., K. Abe, S. Komatsu, K. Sano, N. Yanase and H. Mochizuki. *Novel Ferroelectric Epitaxial BST Capacitor for Deep Sub Micron Memory Applications.* IEEE Electron Device Letters. **18** (11), 529 – 531, 1997.
15. Cha, S.Y., B.T. Jang and H.C. Lee. Effects of Ir Electrodes on The Dielectric Constant of BST Thin Films. Jpn. J. Appl. Phys. **38** (1A), L49 – L51, 1999.
16. Baumert, B.A., L.H. Chang, A.T. Matsuda and C.J. Tracy. A Study of BST Thin Films for Use in bypass Capacitors. J. Mater. Res. **13** (1), 197 –204, 1998.
17. Cheng, J.G., J. Tang and J.H. Chu. Pyroelectric Properties in Sol-Gel Derived BST Thin Films Using a Highly Diluted Precursor Solution. Appl. Phys. Lett. **77** (7), 1035 – 1037, 2000.
18. Vargas, S., R. Arroyo, E. Hari and R. Rodriguez. Effects of Cationic Dopant on The Phase Transition Temperature of Titania Prepared by The Sol-Gel Method. J. Mater. Res., **14** (10), 3932 – 3937, 1999.
19. Wang, F., A. Uusimaki and S. Leppavuori. BST Ferroelectric Film Prepared with Sol-Gel Process and Its Dielectric Performance in Planar Capacitor Structure. J. Mater. Res. **13** (5), 1243 – 1248, 1998.
20. Yoon, K.H., J.H. Park and J.H. Jang. Solution Deposition Processing and Electrical Properties of $Ba(Ti_{1-x}Sn_x)O_3$ Thin Films. J. Mater. Res. **14** (7), 2933 –2939, 1999.
21. Kim, S., T.S. Kang and J.H. Je. Structural Characterization of Laserr Alblation Epitaxial BST Thin Films on MgO (001) by Synchrotron x-Ray Scattering. J. Mater. Res., **14** (7), 2905 – 2911, 1999.
22. Gao, Y., and S. He. Effect of Precursor and Substrate Materials on Microstructure, Dielectric Properties, and Step Coverage of BST Films Grown by Metalorganic Chemical Vapor Deposition. J. Appl. Phys. **87** (1), 124 – 132, 2000.
23. Momose, S., T. Nakamura and K. Tachibana. Effects of Gas Phase Thermal Decompositions of Chemical Vapor Deposition Source Moleculeson The Deposition of BST Films. Jpn. J. Appl. Phys. **39** (9B), 5384 – 5388, 2000.
24. Frutos, J., A.M. Gonzales, M.C. Duro, F. Lopez, J. Meneses, A.J. de Castro and J. Melendez. New Environmental Infrared Sensors. IEEE Electron Device Letters. 203 – 206, 1998.
25. Lim, S.S. M.S. Han, S.R. Hahn and S.G. Lee. Dielectric and Pyroelectric Properties of $(Ba,Sr,Ca)TiO_3$ Ceramics for Uncolled Infrared Detectors. Jpn. J. Appl. Phys. **39** (8), 4835 – 4838, 2000.
26. Washo, B.D. Reology and Modelling of the Spin Coating Process. IBM Res. Develop. 190 – 198, 1977.
27. Daughton, W.J. and F.L. Givens. An Investigation of the Thickness Variation of Spun-on Thin Films Commonly Associated with the Semiconductor Industry. J. Electrochem. Soc., 173 – 179, 1982.
28. Meyerhofer, D. Characteristics of Resist Films Produced by Spining. J. Appl. Phys. **49** (7), 3993 – 3997, 1978.
29. Scriven, L.E. Physics and Application Dip Coating and Spin Coating. Mat. Res. Soc. Symp. Proc. **121**, 717 – 729, 1988.

30. Walsh, C.B., and E.I. Franses. Thickness and Quality of Spin Coated Polymers Films by Two Angle Ellisopmeter. Thin Solid Films. **347**, 167 – 177, 1999.
31. Uchino, K. Ferroelectric Devices. Marcel Dekker, Inc. New York. 23, 2000.
32. Ma, C, Dou A, Chen L, Li Y, Tan X, Dong P, Zhang J,Zheng L, Zhang P.A new nondestructive instrument for bulk residual stress measurement using tungsten Kα1 X-ray. Review Of Scientific Instruments. **87**, 1-7, 2016.
33. Hou, Y, Ji X, Zou L, Liu S, Su X. Performance of cement stabilized crushed brick aggregates in asphalt pavement base and subbase applications. Road Materials and Pavement Design 1-16, 2015.
34. Dubey, S, Gubrele D, Rao R M. Standardization of Yogaamruto Rasa by Using Modern Analysis Techniques. **4**, 27-23, 2016.
35. Pawan, R, Shalini P, Sridurga C. Analytical Study of Panchshara Rasa Through XRD, SEM, EDX, and ZP. International Journal of Ayurveda and Pharma Research. **4**, 35-40, 2016.
36. Erinosho, T O, Collins D M, Wilkinson A J,Todd R I, Dunne F P E. Assessment of X-ray Diffraction and Crystal Plasticity Lattice Strain Under Biaxial Loading. International Journal of Plasticity. 1-29, 2016.
37. Yusuf, N Y, Masdar M S, Isahak W N R W, Nordin D, Husaini T, Majlan E H, Rejab S A M, Chew C L. Ionic liquid impregated activated carbon for biohydrogen purification in an adsorption unit. IOP Conference Series: Materials Science and Engineering. 1-12, 2016.
38. Karami, F, Khanmohammadi, Garmarudi. ATR-FTIR spectroscopy and chemometrics application for analytical and kinetics characterization of adsorption of 1-butyl mercaptan (1-butanethiol) on nickel coated carbon nanofibers (CNFS). Bulgarian Chemical Communications. **48**, 51-56, 2016.
39. Jiang, X, Li S, Xiang G, Li Q, Fan L, He L, Gu K. Determination of the acid values of edible oils via FTIR spectroscopy based on the OAH stretching band. Food Chemistry. **212**, 585-589, 2016.
40. Toon, G C, Blavier J, Sung K, Rothman L S, Gordon I E. HITRAN spectroscopy evaluation using solar occulation FTIR spectra. Journal of Quantitative Spectroscopy and Radiative Transfer. **182**, 324-336, 2016.
41. Yogaraksa, T, Hikam, M, Irzaman. Rietveld analysis of ferroelectric $PbZr_{0.525}Ti_{0.475}O_3$ thin films. Ceramics International. **30**, 1483–1485, 2004.
42. Aidi, M. M, Masjkur, M, Siswadi, Pramudito, S, Arif, A, Syafutra, H, Alatas, H and Irzaman. Phase Transformation of Ba0.55Sr0.45TiO3 Tetragonal to Pseudotetragonal Structures and Arima Model for M. , N,XRD Data. International Journal of Statistic and Application. **3** (5): 19-187, 2013.
43. Kar, S, S. Logad, O. P. Choudhary, C. Debnath, S. Verma, and K. S. Bartwal. Preparation of Lithium Niobate Nanoparticles by High Energy Ball Milling and their Characterization. Universal Journal of Material Sciences. **2**, 18–24, 2013.
44. Yue, W, and J. Y. Jian. Crystal Orientation Dependence of Piezoelectric Properties in LiNbO3 and LiTaO3. Optical Materials. **23**, 403–408, 2003.
45. Syuy, A.V, N. V. Sidorov, A. Yu, Gaponov, M. N. Palatnikov, and V. G. Efremenko, Determination of Photoelectric Fields in A Lithium Niobate Crystal by Parametersof Indicatrix of Photoinduced Scattered Radiation. Optik. 124, 5259–5261, 2013.

46. Weidenfelder, A, J. Shi, P. Fielitz, G. Borchardt, K. D. Becker, and H. Fritze. Electrical and Electromechanical Properties of Stoichiometric Lithium Niobate at High-Temperatures. Solid State Ionics. **225**, 26–29, 2012.
47. Bornand, S, I. Huet, J. F. Bardeau, D. Chateigner, and Papet Ph. An Alternative Route for the Synthesis of Oriented LiNbO3 Thin Films. Integrated Ferroelectric. **43**, 51–64, 2002.
48. Shandilya,S, K. Sreenivas, R. S. Katiyar, and V. Gupta. Structural and Optical Studies on Texture LiNbO3 Thin Film on (0001) Sappire. Journal of Engineering and Materials Sciences. **15,** 355–357, 2008.
49. Gopalan and Venkatraman. Handbook of advanced electronic and photonic materials and devices; New York: Crystal Growth, Characterization, and Domain Studies in Lithium Niobate and Lithium. Tantalate Ferroelectrics. 2001.
50. Cabuk, S, and A. Mamedov. A Study of the LiNbO3 and LiTaO3 Absorption Edge. Tr. J. of Physics. **22**, 41–45, 1998.
51. Yue, W, and J. Yi-jian, Crystal orientation dependence of piezoelectric propertiesin LiNbO3 and LiTaO3. Optical Materials. **23,** 403–408, 2003.
52. Wang, R, and S. A. Bhave, Free-standing high quality factor thin-film lithium Niobatemicro-photonic disk resonators. Optical Society of America. 1–6, 2014.
53. Sadani, B, N. Courjal, G. Ulliac, N. Smith, V. Stenger, M. Collet, F. I. Baida, and M. P. Bernal. Enhanced electro-optical lithium Niobatephotonic crystal wire waveguide on a smart-cutthin film. Optical Society of America. **20** (3), 1–8, 2012.
54. Kashit, I, A. A. Soliman, E. M. Sakr, and A. Ratep, Effect of Different Conventional Melt Quenching Technique on Purity of Lithium Niobate (LiNbO3) Nano Crystal Phase Formed in Lithium Borate Glass. Physics. **2,** 207–211, 2012.
55. Milz, S, J. Rensberg, C. Ronning, and W. Wesch, Correlation Between Damage Evolution, Cluster Formation and Optical Properties of Silver Implanted Lithium Niobate. Nuclear Instruments and Methods in Physics Research B**. 286,** 67–71, 2012.
56. Alim, M.A, A. K. Batra, S. Bhattacharjee, and M. D. Anggarwal, Complex Capacitance in the Representation of Modulus of the Lithium Niobate Crystals. Physica B. **406**, 1088–1095, 2011.
57. Andrushchak, A.S, O. V. Yurkevych, O. A. Burry, V. S. Andrushchak, R. S. Kolodiy, I. M. Solskii, D. Calus, and A. Rusek, Spatial Anisotropy of the Linear Electro-Optic Effect in Lithium Niobate Crystals: Analytical Calculations and their experimental verification. Optical Materials. **45,** 42–46, 2015.
58. Twiefel, J and T. Morita, Utilizing Multilayer Lithium Niobate Elements for Ultrasonic Actuators. Sensors and Actuators A. **166,** 78–82, 2011.
59. Burr, G. W, S. Diziain, and M. P. Bernal, Theoretical Study of Lithium Niobate Slab Waveguides for Integrated Optics Applications. Optical Materials**. 31**, 1492–1497, 2009.
60. Liu, M, and D. Xue,. Effect of Heating Rate on the Crystal Composition of Ferroelectric Lithium Niobate Crystallites. Journal of Alloys and Compounds. **427**, 256–259, 2007.
61. Bharath,S, C, K. R. Pimputkar, A. M. Pronschinske, and T. P. Pearl, Liquid CrystalDeposition on Poled, Single Crystalline Lithium Niobate. Applied Surface Science**. 254,** 2048–2053, 2008.
62. Ismon, M.D.S, H. H. Kusuma, and M. R. Sudin, A Study of The Linbo3 Crystal Growth Rocess by the Czochralski Method. Proceedings Sciences and Mathematic Simposium. 1–7, 2005.

63. Petukhov, I.V, V. I. Kichigin, A. P. Skachkov, S. S. Mushinsky, D. I. Shevtsov, and A. B. Volyntsev, Microindentation of Proton Exchange Layers on X Cut of Lithium Niobate Crystals. Materials Chemistry and Physics. **135,** 493–496, 2012.
64. Box, George; Jenkins, Gwilym (1970). Time Series Analysis: Forecasting and Control. San Francisco: Holden-Day.
65. Liu, K., Chen Y. and Zhang X. An Application of the Seasonal Fractional ARIMA model to the Semiconductor Manufacturing. IFAC Papers Online. **50**-1,8097-8102, 2017.
66. Sen, P, Roy M and Pal P. Application of ARIMA for forecasting energy consumption and GHG emission: A case study of an indian pig iron manufacturing organization. Energy, 1031-1038, 2016.
67. Zafra, C, Angel Y and Torres E. ARIMA analysis of the effect of land surface coverage on PM10 concentrations in a high-altitude megacity. Atmospheric Pollution Research, 1-9, 2017.
68. Yuan, C, Liu S and Fang Z. Comparison of China's primary energy consumption forecasting by using ARIMA and GM model. 2016, 384-390. 2016.
69. Jeyasekar, A, Raja SVK and Uthra RA. Congestion Avoidance Algorithm Using ARIMA Model-Based RTT in Heterogeneous Wired-Wireless Networks. Journal of Network and Computer Application. 1-42, 2016.
70. Oliveira, PJ, Steffen JL and Cheung P. Parameter Estimation of Seasonal Arima Models for Water Demand FOrecasting using the Harmony Search Algorithm Procedia Engineering, Vol. **186**, 177-185, 2017.
71. Koutroumanidis, T, Ioannou K, Arabatzis Garyfallos. Predicting fuelwood pricesin Greece with the use of ARIMA models, artificial neural network and hybrid ARIMA-ANN model. Energy Policy. **37**, 3627-3634, 2009
72. Qin, M, Li Z. and Du Z. Red tide time series forecasting by combining ARIMA. Knowledge-Based Systems, 1-24, 2017.